The effects of resolving the Canadian Arctic Archipelago in a finite element sea ice model

Olivier Lietaer[a,b,*], Thierry Fichefet[b], Vincent Legat[a]

[a] Centre for Systems Engineering and Applied Mechanics (CESAME),
Université catholique de Louvain. 4, Avenue G. Lemaître. B-1348 Louvain-la-Neuve, Belgium.

[b] G. Lemaître Institute of Astronomy and Geophysics (ASTR),
Université catholique de Louvain. 2, chemin du Cyclotron. B-1348 Louvain-la-Neuve, Belgium.

July 12, 2009

Manuscript submitted for publication in *Ocean Modelling* on January 15, 2008

Abstract

Though narrow straits may have a strong influence on the large-scale sea ice mass balance, they are often crudely represented in coarse resolution sea ice models. Unstructured meshes, with their natural ability to fit boundaries and locally increase the mesh resolution, propose an alternative framework to capture the complex oceanic areas formed by coasts and islands. In this paper, we develop a finite element sea ice model to investigate the sensitivity of the Arctic sea ice cover features to the resolution of the narrow straits constituting the Canadian Arctic Archipelago. The model is a two-level dynamic-thermodynamic sea ice model, including a viscous-plastic rheology. The model is run over 1979-2005, forced by daily NCEP/NCAR reanalysis data. Confronting qualitatively numerical experiments with observations shows a good agreement with satellite and buoys measurements. Due to its simple representation of the oceanic interactions, the model overestimates the sea ice extent during winter in the southernmost parts of the Arctic, while the Baffin Bay and Kara Sea remain ice-covered during summer. Advantages of unstructured meshes include a better representation of shelf water polynyas thanks to an increased mesh resolution near the coastlines. In order to isolate the benefits from resolving the Canadian Archipelago, a numerical experiment is performed where we artificially close the Archipelago. Focusing on the large-scale sea ice thickness pattern, no significant change is found in our model, except in the close surroundings of the Archipelago. However, the local and short-term influences of the ice exchanges are nonnegligible. In particular, we show that the ice volume associated to the Canadian Archipelago represents 10 % of the Northern Hemisphere sea ice volume and that the annual mean ice export towards Baffin Bay amounts to 125 km^3 yr^{-1}, which may play an important role on the convective overturning in the Labrador Sea.

Keywords: Sea ice model, Unstructured mesh, Finite element method, Canadian Archipelago

1 Introduction

Sea ice is a key component of the high latitudes climate (e.g., *Serreze et al.*, 2007). In regions where the incoming solar radiation at the top of the atmosphere is higher during local summer than elsewhere on Earth (e.g., *Wallace and Hobbs*, 1977), most of the downwelling shortwave radiation is reflected due to the high snow and ice albedos (e.g., *Perovich et al.*, 2002). Moreover, the salt rejected into the underlying water during sea ice formation plays a crucial role in the

*Corresponding author. E-mail: olivier.lietaer@uclouvain.be, Tel: +32 10 47 23 57, Fax: +32 10 47 21 80

formation of convection and thus in the global thermohaline circulation (e.g., *Aagaard and Carmack*, 1989). Sea ice further constitutes a natural barrier between the atmosphere and ocean, insulating the relatively warm ocean waters from the cold atmosphere by drastically limiting mutual heat, momentum and water mass exchanges. All these interactions illustrate the complex role played by sea ice in the climate system. In particular, the ice-albedo feedback (*Ebert and Curry*, 1993) is considered to be largely responsible for the high sea ice sensitivity to climate change, as highlighted by simulations with climate general circulation models (CGCMs) on the one hand (e.g., *Manabe and Stouffer*, 1980), and by the recent Arctic sea ice minima of extent on the other hand (*Stroeve et al.*, 2005). Nevertheless, recent comparisons (e.g., *Holland and Bitz*, 2003; *Arzel et al.*, 2006; *Zhang and Walsh*, 2006; *Lefebvre and Goosse*, 2008) between CGCM simulations plead for the need to improve our understanding of sea ice and its representation in climate models.

Sea ice is drifting on the ocean, mainly driven by the wind and the ocean currents. The large-scale Arctic ice circulation is characterized by two main features. In the western part of the Arctic, the ice describes a large anticyclonic gyre named the Beaufort Gyre where the ice can be trapped for up to 10 years (*Hibler*, 1980), with typical ice velocities of 2 cm s^{-1}. In the east, the ice is transported by the Transpolar Drift from the north of Siberia to the North Atlantic through Fram Strait. This strait is approximately 435 km wide and constitutes the main exit for the Arctic sea ice, the ice volume export reaching about 2200 km^3 yr^{-1} (*Kwok et al.*, 2004). Narrow straits, on their part, may have a strong impact on the geophysical flows in general (e.g. water mass exchanges between different oceanic basins, complex flow in localized areas, etc.) and in the polar regions they can be responsible for a somewhat chaotic dynamical behavior of sea ice. Due to the high ice concentration and low ice temperature, the formation of ice bridges in channels like Nares Strait (*Samelson et al.*, 2006) may prevent any ice flow for several months. Later, the ice is suddenly released when the plugs collapse. Moreover, the ice characteristics in these channels have a strong interannual variability (*Melling*, 2002; *Kwok*, 2006).

Of particular concern is the complex area formed by the numerous islands and coastlines in the Canadian Arctic Archipelago (CAA). The straits constitute an important pathway for the cold waters from the Arctic Ocean to the Atlantic. Even if many recent studies have explored the freshwater cycle of the Arctic (e.g., *Stigebrandt*, 2000; *Serreze et al.*, 2006), large uncertainties remain, especially concerning the sea ice contribution. Assembling different sources, we get the following picture: estimates of the ice freshwater outflow through the southern part of the CAA roughly amount to 160 km^3 yr^{-1} (*Prinsenberg and Hamilton*, 2005), while, in the north, the Nares Strait sea ice flux (*Kwok et al.*, 2004) accounts for $\sim$ 100 km^3 yr^{-1} of freshwater (assuming a sea ice salinity of 4 psu for a reference seawater salinity of 34.8 psu, and a density of 900 kg m^{-3}, see *Serreze et al.* (2006)). In comparison, the oceanic freshwater flux through the CAA is evaluated by *Prinsenberg and Hamilton* (2005) at 3200 km^3 yr^{-1}. The rest of the northern gates of the CAA contributes to a net inflow into the Arctic (*Kwok*, 2006), suggesting as stated in the latter study that most of the ice exported into Baffin Bay (except from Nares Strait) is produced in the CAA rather than exported from the Arctic. Because sea ice is landfast during a large part of the year in the northern CAA (*Melling*, 2002), the different straits act as a "buffer" on sea ice between the Arctic Ocean and Labrador Sea, preventing Arctic ice outflow in the north and providing ice generation (*Sou*, 2007) in the south.

The role of the freshwater flux through the CAA is thought to be important regarding the freshwater budget of the region (*Stigebrandt*, 2000; *Dickson et al.*, 2007), and may play an important role on the convective overturning in the Labrador Sea (*Goosse et al.*, 1997a). Less known is the influence of the ice contribution to this freshwater export on the one hand, and the potential link with the troubles shown by most of the models to simulate the decay of the summer sea ice cover in Baffin Bay on the other hand (*Timmermann et al.*, 2005; *Johnson et al.*, 2007; *Vancoppenolle et al.*, subm.). Finally, data in this harsh region of the world are scarce (e.g., *Melling*, 2002), especially concerning the ice thickness, ranging between 2 and 6 m in the CAA

(*Bourke and Garrett*, 1987; *Melling*, 2002; *Kwok*, 2005), underlining the need for numerical experiments. Furthermore, this area is currently being of strong economical importance and political interest in the context of the opening of the Northwest Passage.

Finite element methods have been proposed at the onset of sea ice modeling. In the framework of the AIDJEX project (Arctic Ice Dynamics Joint Experiment), *Mukherji* (1973) was the first to make use of a finite element method code for its aptitude to simulate the crack propagation in sea ice. A few years later, *Becker* (1976) introduced the guiding lines of the method and asserted: "*Because of their generality and widespread use, finite element techniques seem a worthwhile alternative to the difference scheme. [...] The ease with which finite element techniques can be used to model complicated shapes with arbitrary variation in the mesh spacing is likely to be the motivating factor leading to any such use.*". In the early eighties, *Sodhi and Hibler* (1980) used in a pioneer study an unstructured grid along with a finite element method in order to resolve the ice drift in the complex region of Strait of Belle Isle. Another work investigating the finite element method in sea ice modeling was held by *Thomson et al.* (1988). They performed a comprehensive comparison between different constitutive laws for Eulerian and Lagrangian decriptions in order to model the short-term ice motion in Beaufort Sea.

Unstructured grids have among others the advantage to avoid the pole singularity and related stability problems (*Williamson*, 1979) and to represent in a more accurate fashion coastlines (e.g., *Adcroft and Marshall*, 1998; *Legrand et al.*, 2006). Recently, many efforts have been brought to investigate the contribution of unstructured meshes in ocean modeling (e.g., *Walters*, 1992; *Lynch et al.*, 1996; *Le Roux et al.*, 2000; *Danilov et al.*, 2004; *Pietrzak et al.*, 2005; *White et al.*, 2008a) and in sea ice modeling (*Schulkes et al.*, 1998; *Yakovlev*, 2003; *Wang and Ikeda*, 2004; *Sulsky et al.*, 2007). Very few modeling research has been performed on the CAA. Two studies are based on unstructured grid regional models: *Kliem and Greenberg* (2003) constructed gridded fields of potential temperature and salinity, used in a second step to simulate the mean circulation in the area, while *Sou* (2007) studied the impact of future climate scenarios on the CAA. The present paper in turn presents a large-scale sea ice model operational for climate studies which, to the authors' knowledge, is the first to investigate the effects of resolving the CAA on the ice cover features.

The model presented is aimed to be coupled to the finite element ocean model SLIM[1] (*White et al.* (2008b)). As both models are still under development, and because a large part of the variability of the ice circulation can be explained by the winds (*Thorndike and Colony*, 1982; *Serreze et al.*, 1989), the studies presented here are run with an uncoupled sea ice model with no ocean dynamics. Furthermore, the ocean stress in not significant in most of the northern CAA due to the weak ocean currents (*Stronach et al.*, 1987). The sea ice model includes a viscous-plastic rheology and the *Semtner* (1976) zero-layer thermodynamic scheme. It is evident that some distance must be taken while analyzing the model results because of the simple thermodynamics used and the absence of ocean currents. The model complexity is nevertheless found sufficient for the purpose of this paper is to focus (i) on the feasibility and advantages of unstructured grids in large-scale sea ice modeling, and (ii) on the main trends of the influence of the CAA on the Arctic ice cover and freshwater budget.

This paper is organized as follows. Section 2 describes the sea ice model, while Section 3 deals with its numerical resolution and focuses on its finite element implementation. In Section 4, the model results are first confronted to the observations in order to validate the model. The influence of the CAA resolution on the results is then investigated via sensitivity experiments. Concluding remarks are finally given in Section 5.

[1]Second-generation Louvain-la-Neuve Ice-ocean Model, `http://www.climate.be/SLIM`.

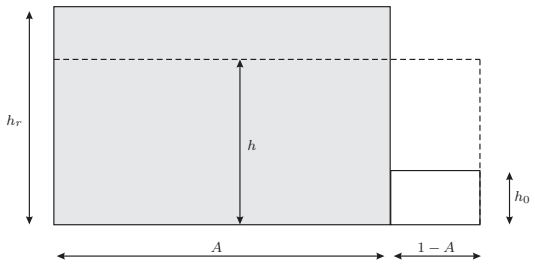

Figure 1: Two-level model: neglecting h_0 leads to a simplified relation between mean (h) and actual (h_r) ice thicknesses: $h = Ah_r$.

2 Model description

Following *Hibler* (1979), sea ice is assumed to behave dynamically as a viscous-plastic fluid with nonlinear viscosities. The model includes two thickness categories (see Fig. 1): thick ice with an actual mean thickness h_r and thin ice corresponding to a thickness lower than a cutoff constant h_0. In this so-called two-level model, we introduce two variables to describe sea ice on a parcel: the mean ice thickness h and the ice concentration A, which is defined as the proportion of thick ice recovering the parcel. The relation between those variables is illustrated in Fig. 1.

According to the aforementioned definitions, the equation of momentum conservation reads:

$$\rho h \frac{D\boldsymbol{u}}{Dt} = -\rho h f \boldsymbol{k} \times \boldsymbol{u} + A\left(\boldsymbol{\tau}_a + \boldsymbol{\tau}_w\right) - \rho h g \boldsymbol{\nabla}\xi + \boldsymbol{\nabla}\cdot\boldsymbol{\sigma} \tag{1}$$

where ρh is the ice mass per unit area, $\boldsymbol{u}$ the ice velocity, $\frac{D}{Dt} = \frac{\partial}{\partial t} + \boldsymbol{u}\cdot\boldsymbol{\nabla}$ is the material derivative, f the Coriolis parameter (taken to be constant for the high latitudes), $\boldsymbol{k}$ is a unit vector normal to the surface, $\boldsymbol{\tau}_a$ et $\boldsymbol{\tau}_w$ are respectively the air and ocean surface stresses on the ice weighed by the ice concentration (*Connolley et al.*, 2004), g the acceleration due to gravity, ξ the sea surface dynamic height and $\boldsymbol{\sigma}$ the ice internal stress tensor. Both the air and water stresses are parameterized by quadratic drag laws, the water stress depending on the ice velocity:

$$\boldsymbol{\tau}_w \quad = \quad \rho_w C_w \left|\boldsymbol{U}_w - \boldsymbol{u}\right| \left[\left(\boldsymbol{U}_w - \boldsymbol{u}\right)\cos\theta_w + \boldsymbol{k}\times\left(\boldsymbol{U}_w - \boldsymbol{u}\right)\sin\theta_w\right] \tag{2}$$

where C_w is the water drag coefficient, ρ_w the water density and θ_w the water turning angle. The force due to the ocean tilt is commonly computed by establishing the geostrophic balance with the ocean current:

$$-\rho h g \boldsymbol{\nabla}\xi = \rho h f \boldsymbol{k} \times \boldsymbol{U}_w \tag{3}$$

In our model, the ocean velocity $\boldsymbol{U}_w$ is uniformly equal to zero, hence reducing the water surface stress to a simple drag of the ocean on the ice. Additionally, the contribution of the ocean tilt is neglected. We shall nevertheless take these terms into account in the rest of this paper for the sake of generality.

The viscous-plastic rheology assumes that sea ice is behaving as a nonlinear compressible viscous fluid with the general form:

$$\boldsymbol{\sigma} = 2\eta\left(\dot{\boldsymbol{\epsilon}}, P\right)\dot{\boldsymbol{\epsilon}} + \Big(\zeta\left(\dot{\boldsymbol{\epsilon}}, P\right) - \eta\left(\dot{\boldsymbol{\epsilon}}, P\right)\Big)\mathrm{tr}\left(\dot{\boldsymbol{\epsilon}}\right)\boldsymbol{I} - \frac{P}{2}\boldsymbol{I} \tag{4}$$

where $\dot{\boldsymbol{\epsilon}} = \frac{1}{2}\left(\boldsymbol{\nabla}\boldsymbol{u} + \boldsymbol{\nabla}\boldsymbol{u}^T\right)$ is the strain rate tensor, $\boldsymbol{I}$ the identity tensor, η and ζ are the shear and bulk viscosities, respectively, and P the pressure. For normal strain rates, ice is assumed to behave plastically, while for small strain rates ice is supposed to flow very slowly in a viscous way. In the one-dimensional case, the yield delimiting the plasticity state from the creep flow corresponds to a fixed strain rate $\dot{\epsilon}_0$. In two dimensions, this yield stress concept is generalized through a yield curve in the principal stress plane. If the stress state lies inside this curve,

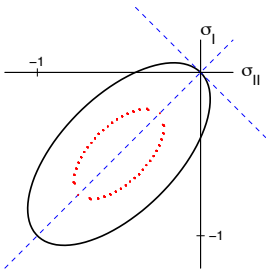

Figure 2: Representation of material points for which $0.965 \times 10^{-9} \leq \gamma \leq 10^{-9}$ s^{-1} (red) plotted in a principal stress space. The material points yielding a $\gamma \geq 2 \times 10^{-9}$ s^{-1} lie on the ellipse and undergo hence plastic deformation (solid line).

ice behaves viscously; otherwise, ice is constrained to plasticity and the state lies on the curve. *Hibler* (1979)'s original elliptical yield curve has been widely used, and, combined to the normal flow rule, it yields the following viscosities:

$$\zeta = \min\left(\frac{P}{2\gamma}, 2.5 \times 10^8 P\right) \quad \text{and} \quad \eta = \zeta/e^2 \tag{5}$$

where e is the ellipse eccentricity (typically 2), P is the ice strength, determining the ellipse size, and γ is given by :

$$\gamma = [(\dot{\epsilon}_{xx}^2 + \dot{\epsilon}_{yy}^2)(1 + 1/e^2) + 4\dot{\epsilon}_{xy}^2/e^2 + 2\dot{\epsilon}_{xx}\dot{\epsilon}_{yy}(1 - 1/e^2)]^{1/2} \tag{6}$$

and can be interpreted as a measure of the strain rate determining whether the material undergoes plastic deformation or not. In the principal stress plane, all the stress states characterized by the same γ value lie on an ellipse centered on $(-1/2, -1/2)$ whose size normalized by P is proportional to γ (Fig. 2). Finally, we need an expression of the pressure term to close the system. Following *Hibler* (1979), P is set proportional to h and A:

$$P = p^* \, h \, e^{-C(1-A)} \tag{7}$$

with two empirical parameters p^* and C.

Mass conservation is ensured by an advection equation for the mean ice thickness, while another continuity equation is required for the ice concentration:

$$\frac{\partial h}{\partial t} + \boldsymbol{\nabla} \cdot (\boldsymbol{u}h) = S_h \tag{8}$$

$$\frac{\partial A}{\partial t} + \boldsymbol{\nabla} \cdot (\boldsymbol{u}A) = S_A \tag{9}$$

where S_h and S_A are source terms accounting for sea ice ablation or accretion. In addition, the ice concentration is constrained ($A \leq 1$) to roughly account for the mechanical redistribution of sea ice. Inspired by *Thomson et al.* (1988), the redistributed values of the actual ice thickness h'_r and concentration A' are given by:

$$h'_r = h_r + h_r[A - 1]^+,$$

$$A' = A - [A - 1]^+,$$

where $[f]^+$ is the positive part of f, i.e. $\max(f, 0)$. This formulation clearly shows a source term for h_r and a sink term for A: the idea here is to prevent the ice concentration to exceed unity while the actual ice thickness is allowed to increase.

The computation of heat diffusion within the thick ice is based on *Semtner* (1976)'s zero-layer model. This model neglects the storage of sensible and latent heat, resulting in a linear temperature profile in the ice. Following *Fichefet et al.* (1998), two boundary conditions are needed, expressed as a heat budget at the surface (giving the possible ablation rate $S_{h_r}^{su}$ of the actual ice thickness) and at the bottom of the ice ($S_{h_r}^{b}$). The term S_h is hence made of two contributions:

$$S_h = A\,(S_{h_r}^{su} + S_{h_r}^{b}).$$

At the upper surface, an equilibrium surface temperature T_s is computed from the heat balance:

$$\underbrace{(1-\alpha)F_r + F_L + F_s + F_l}_{F_A} + F_C = 0,$$

where α is the surface albedo, which in our model is prescribed for each month and takes the presence of snow into account. F_A is the net atmospheric flux to the upper ice surface and F_C is the conductive flux through ice. Fluxes directed to the ice surface are taken to be positive. In order to solve the heat balance equation, the model includes a parameterization of the solar radiation F_r (*Zillmann*, 1972), the net longwave radiation F_L (*Berliand and Berliand*, 1952) and turbulent fluxes of sensible F_s and latent F_e heat (classical bulk formulae, see *Goosse* (1997b)). If the predicted temperature T_s is above the melting point, its value is reduced to that point, yielding an excess of energy counterbalanced by latent heat absorption:

$$S_{h_r}^{su} = -\frac{F_A + F_C}{L_i},$$

with L_i the volumetric latent heat of fusion of ice.

At the base of the ice, the bottom temperature is kept at the freezing point of seawater. The melting or growth rate of the ice depends only on the conductive heat flux and the oceanic heat flux F_b:

$$S_{h_r}^{b} = \frac{F_C - F_b}{L_i}.$$

We assume that the ocean has a constant mixed layer depth $h_{mxl} = 30$ m. This ocean layer is characterized by a unique temperature (T_w) that is equal to the freezing point of the seawater (T_f) if there is ice on the parcel. The oceanic flux consists of a restoring term towards a climatological temperature of the mixed layer (T_{mxl}) taken from the Polar science center Hydrographic Climatology (PHC 3.0, updated from: *Steele et al.* (2001)):

$$F_b = \rho_w\, C_{pw}\, h_{mxl}\, \gamma_t\, (T_{mxl} - T_w)\,, \tag{10}$$

where C_{pw} is the specific heat of seawater and γ_t a relaxation constant.

In the case of thin ice and open water, another heat budget B_l is computed to account for lateral growth or decay:

$$B_l = (1-\alpha_w)F_r + F_L + F_s + F_l + F_b,$$

where α_w stands for the ocean surface albedo. If B_l is negative, the lead is partially filled with ice of thickness h_0 (*Fichefet et al.*, 1998):

$$S_A^{acc} = -\frac{(1-A)B_l}{L_i h_0}.$$

When the heat balance is positive, the lateral decay on its turn is computed as:

$$S_A^{ab} = -\frac{A}{2h}[-S_h]^+.$$

Finally, the different data sets used to run the model are daily NCEP/NCAR reanalysis data for the air temperature and the wind velocity, and monthly climatologies for the relative humidity (*Trenberth et al.*, 1989) and the total cloudiness (*Berliand and Strokina*, 1980).

3 Numerical method

In this section, the equations and the initial and boundary conditions of the sea ice model are presented. The finite element spatial discretization of this boundary value problem is derived and the system of equations obtained is integrated with respect to time.

The sea ice model consists in finding the ice velocity $\boldsymbol{u}(t,x,y)$, the mean ice thickness $h(t,x,y)$ and the ice concentration $A(t,x,y)$ satisfying the following partial differential equations:

$$\begin{aligned} \rho h \frac{\partial \boldsymbol{u}}{\partial t} &= \boldsymbol{\nabla}\cdot\boldsymbol{\sigma}(\boldsymbol{u},h,A) + \boldsymbol{S_u}(\boldsymbol{u},h,A) \\ \frac{\partial h}{\partial t} + \boldsymbol{\nabla}\cdot(\boldsymbol{u}h) &= S_h(h,A) \\ \frac{\partial A}{\partial t} + \boldsymbol{\nabla}\cdot(\boldsymbol{u}A) &= S_A(h,A) \end{aligned}$$

on the two-dimensional domain Ω englobing the whole Arctic sea ice north of the parallel 50 degrees North. In the momentum equation, the term $\boldsymbol{S_u}$ takes into account the wind and ocean forcings, the Coriolis force and the force due to the tilt of the ocean, and the advection has been neglected (*Fichefet et al.*, 1998) in the momentum balance (Eq. (1)). All the calculations are performed from a given initial situation where all fields are specified. The kind of boundary conditions is twofold: on the one hand, a no-slip condition is prescribed along the coastline and islands. On the other hand, along the open sea boundary, a stress-free boundary condition is applied, while the inward ice thickness and concentration fluxes are prescribed.

The finite element method consists of three major steps.

- We divide the domain Ω into a triangulation of non overlapping elements Ω_e as shown in Fig. 3. Unstructured grids enable a flexible distribution of the degrees of freedom in the domain according to the areas of interest. Hence, in this study, large elements are used far from the shelf and in areas of low latitudes where few ice is observed, while the mesh is refined along coastlines, especially in the CAA.

- We replace the three unknown fields by some piecewise polynomial approximations defined as follows:

$$\begin{aligned} \boldsymbol{u}(t,x,y) &\approx \boldsymbol{u}^h(t,x,y) = \textstyle\sum_{j=1}^{p} \boldsymbol{U}_j(t)\phi_j(x,y) \\ h(t,x,y) &\approx h^h(t,x,y) = \textstyle\sum_{j=1}^{m} H_j(t)\psi_j(x,y) \\ A(t,x,y) &\approx A^h(t,x,y) = \textstyle\sum_{j=1}^{m} A_j(t)\psi_j(x,y) \end{aligned}$$

  where the shape functions ϕ and ψ are defined a priori and $\boldsymbol{U}_j(t)$, $H_j(t)$ and $A_j(t)$ are the nodal unknowns. The local support of those polynomial shape functions is the key ingredient of the finite element method allowing us to derive a discrete algebraic system enjoying nice sparsity properties.

- Finally, we define a discrete Galerkin formulation to obtain numerical values for the nodal unknowns. Such a procedure imposes that the weighted residuals of the partial differential equations have to vanish. Typically, we integrate over the whole domain the partial differential equations weighted by the shape functions. However, even if those residuals vanish, it does not ensure that the differential equations will be satisfied everywhere by

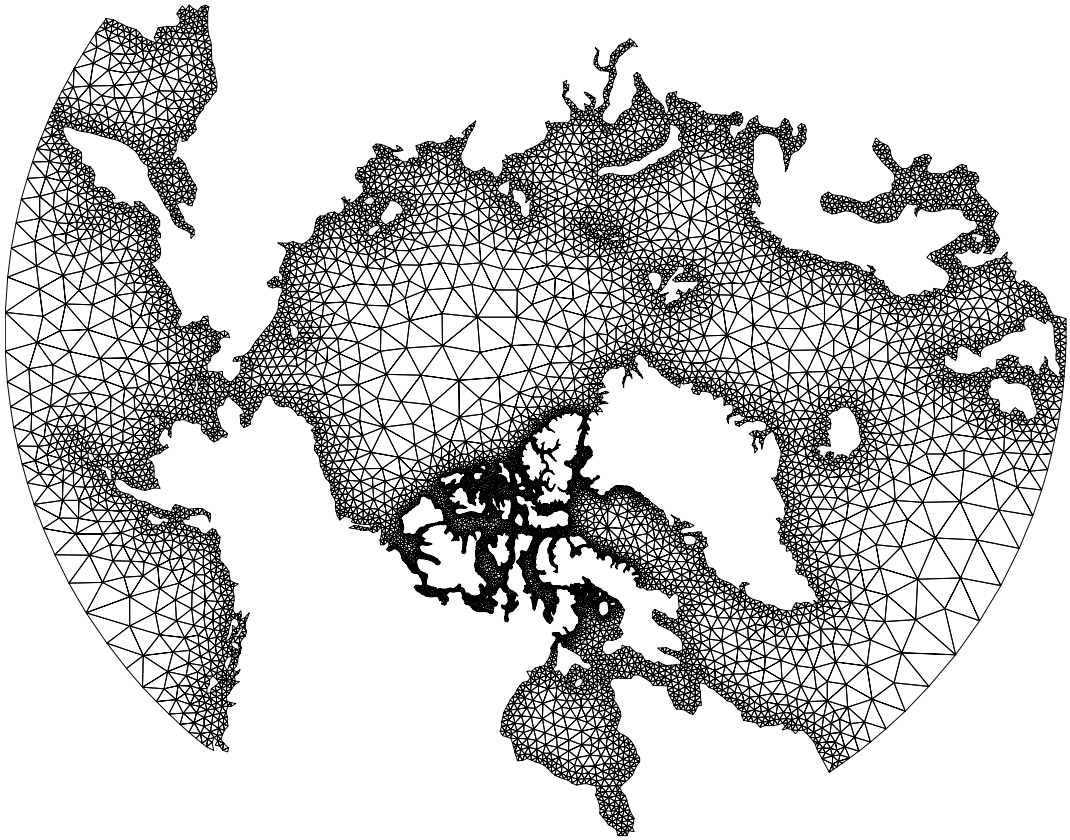

Figure 3: Finite element mesh of the Arctic. The domain extends north of the parallel 50 degrees North. The mesh resolution varies from 10 to 400 km.

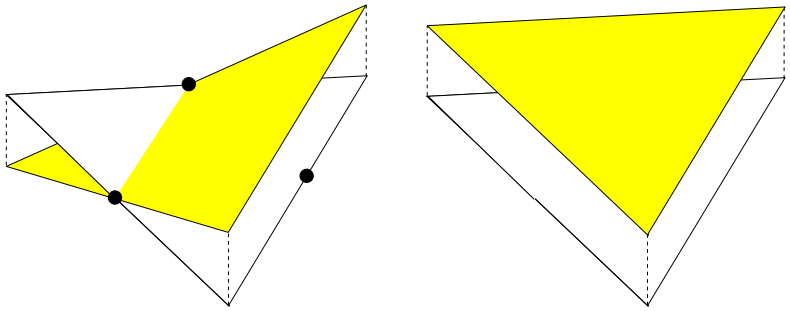

Figure 4: Linear nonconforming (left) and constant (right) shape functions.

$\boldsymbol{u}^h$, h^h and A^h. Moreover, some integrals by parts are performed in order to reduce the degree of differenciability required by the shape functions. One clear advantage of the finite element method for sea ice modeling is its facility to handle boundary conditions (*Thomson et al.*, 1988). Taking advantage of the homogeneous stress boundary condition, the spatial discretization reads:

Find $\boldsymbol{u}^h$, h^h and A^h such that:

$$< \phi_j \rho h^h \frac{\partial \boldsymbol{u}^h}{\partial t} > \;=\; - < \boldsymbol{\nabla}\phi_j \cdot \boldsymbol{\sigma}^h > + < \phi_j A^h \boldsymbol{S_u}(\boldsymbol{u}^h, h^h, A^h) > \qquad j = 1, \ldots, p$$

$$< \psi_j \frac{\partial h^h}{\partial t} > \;=\; < \boldsymbol{\nabla}\psi_j \cdot \left(\boldsymbol{u}^h h^h\right) > - \ll \psi_j h^h \left(\boldsymbol{u}^h \cdot \boldsymbol{n}\right) \gg + < \psi_j S_h(h^h, A^h) > \qquad j = 1, \ldots, m$$

$$< \psi_j \frac{\partial A^h}{\partial t} > \;=\; < \boldsymbol{\nabla}\psi_j \cdot \left(\boldsymbol{u}^h A^h\right) > - \ll \psi_j A^h \left(\boldsymbol{u}^h \cdot \boldsymbol{n}\right) \gg + < \psi_j S_A(h^h, A^h) > \qquad j = 1, \ldots, m$$

where $\boldsymbol{n}$ denotes the outward normal, the notation $< \, . \, >$ holds for $\int_\Omega \, . \, d\Omega$ and $\ll \, . \, \gg$ for $\int_{\partial\Omega} \, . \, d\Gamma$.

This spatial discretization leads to a nonlinear system at each time step whose unknowns are the nodal values. A nonconforming linear approximation (*Hua and Thomasset*, 1984) is chosen for the velocity field, while the mean ice thickness and concentration are approximated by constant shape functions (Fig. 4). The two-level model proposed by *Hibler* (1979) suggests indeed a constant mean ice thickness and concentration in each cell, even if not excluding a higher order representation of both variables. Advantages of the linear nonconforming elements include an easier computation of the fluxes through the edges and the orthogonality of the shape functions. In the set of discrete equations, it is important to emphasize that the integral on the domain has to be splitted as the sum of the integrals on each element because the derivative no longer exists on the edge. This is so because nonconforming shape functions are discontinuous across elements edges. In the same way, the boundary integral is now the sum of the integrals along all internal and external edges. For more details, we refer to *Hanert et al.* (2004). Finally, we perform a hybrid time scheme where Coriolis force and external forcings due to the ocean are implicitly integrated. To take into account nonlinear terms, a standard linearization based on a Newton-Raphson scheme is introduced, and the resulting sparse matrix is solved with a "skyline" linear solver. Typically, for a simple Euler scheme, the discrete equations read:

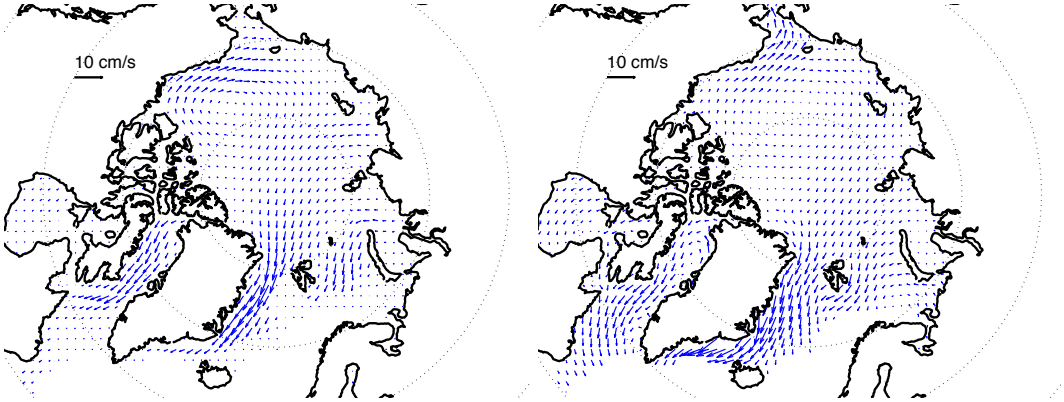

Figure 5: Mean climatological ice drifts (1979-2005). Left: observations; right: the velocity field is computed by our model. Both fields have been interpolated on a regular grid for visual convenience.

$$
\begin{aligned}
< \phi_j \rho h_n^h \left(\boldsymbol{u}_{n+1}^h - \boldsymbol{u}_n^h\right) > &= \Delta t \left(- < \boldsymbol{\nabla}\phi_j \cdot \boldsymbol{\sigma}_n^h > + < \phi_j \boldsymbol{S}_{\boldsymbol{u}}^h(\boldsymbol{u}_{n+1}^h, h_n^h, A_n^h) > \right) \\
< \psi_j \left(h_{n+1}^h - h_n^h\right) > &= \Delta t \left(- \ll \psi_j h_n^h \left(\boldsymbol{u}_{n+1}^h \cdot \boldsymbol{n}\right) \gg + < \psi_j S_h(h_n^h, A_n^h) > \right) \\
< \psi_j \left(A_{n+1}^h - A_n^h\right) > &= \Delta t \left(- \ll \psi_j A_n^h \left(\boldsymbol{u}_{n+1}^h \cdot \boldsymbol{n}\right) \gg + < \psi_j S_A(h_n^h, A_n^h) > \right)
\end{aligned}
$$

where the subscript denotes the time evaluation.

Advection is computed via a first-order, finite volume upwind-weighted scheme. Though numerically diffusive, it is monotonic and conservative, two essential ingredients to ensure the positive-definiteness of the transported variables h and A.

4 Results and discussion

The model has been run over the period 1979-2005. We first present results from the control simulation, essentially focusing on the patterns of ice concentration, mean ice thickness and ice drift. A special attention is paid to the ability of the model to represent the formation of coastal polynyas thanks to the flexibility of unstructured grids. A numerical experiment is further presented where we investigate the influence of the ice flow through the narrow straits of the CAA on the Arctic ice thickness distribution and freshwater budget.

4.1 Control run

The model is spun up for only 6 years with annual mean forcings and then integrated with daily wind and air temperature forcings between 1979 and 2005. The mesh used for this simulation has a varying resolution between 10 km in the CAA and 400 km (Fig. 3).

We first compare the annual mean sea ice drifts simulated during the whole 1979-2005 period to the available data (Fig. 5). The daily observed ice motion vectors for the 1979-2005 period are derived from data of Advanced Very High Resolution Radiometer (AVHRR), Scanning Multichannel Microwave Radiometer (SMMR), Special Sensor Microwave/Imager (SSM/I), and International Arctic Buoy Programme (IABP) (http://nsidc.org, *Fowler* (2003)). The simulated ice drift vectors are only represented on grid points where the annual mean ice concentration is higher than 15%, a value that will be considered here as delimiting the ice edge.

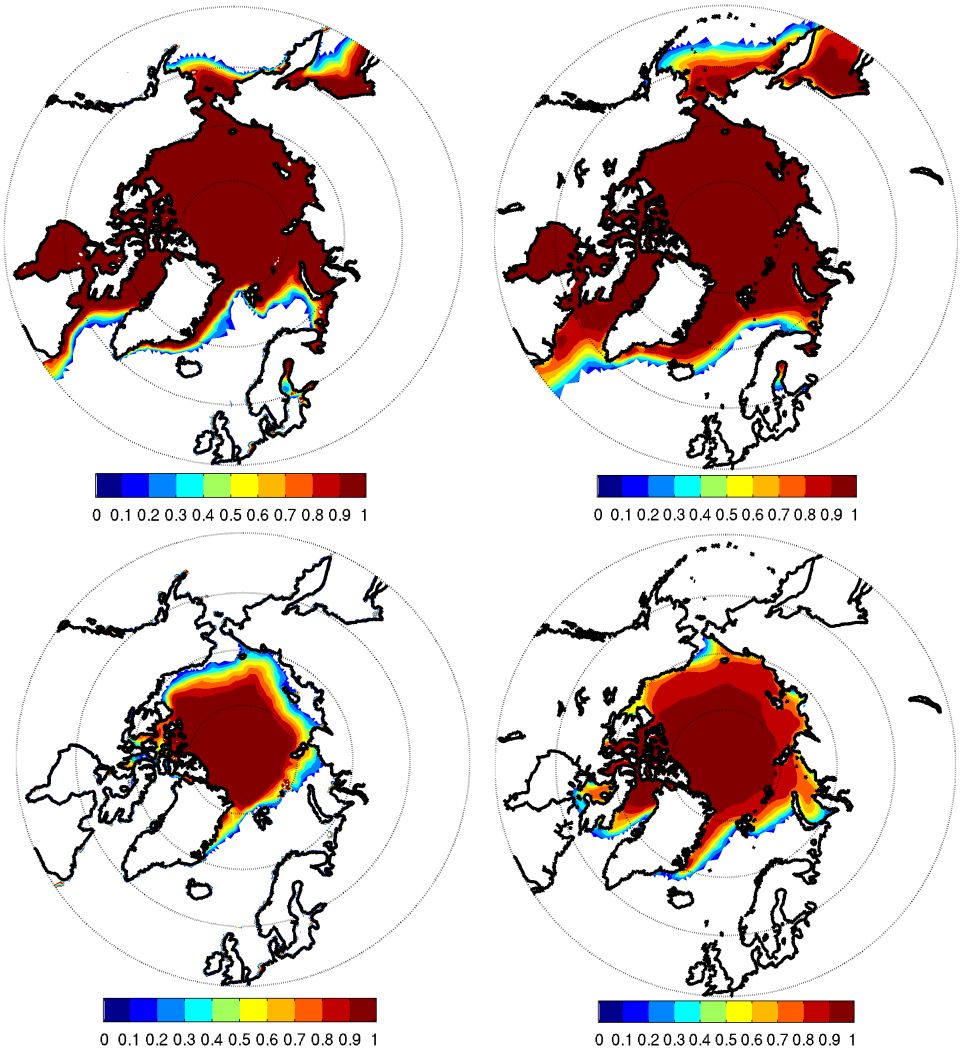

Figure 6: Mean ice concentrations in March (top) and September (bottom). For both months, we compare the data sets (left, 1979-2005) derived from SMMR and SSM/I and interpolated on the finite element grid with the simulated ice concentrations (right, 1979-2005).

Both the Beaufort Gyre and the Transpolar Drift Stream are recognizable in the observations and the simulation, attesting that the model captures well the essential of the ice circulation in the Arctic. However, the simulated Beaufort Gyre appears weakened and the model is clearly missing the ice flow in the region of Bering Strait: on a climatological time scale, observations suggest that the ice is almost static there, while the model exhibits a clear ice outflow from the Arctic. This difference is attributed to the oceanic surface currents flowing from the North Pacific to the Arctic Basin through Bering Strait that should thus counterbalance the wind stress. The simulated ice dynamics indicates also a higher ice drift along the east coast of Greenland, while a parabolic-like velocity profile across Fram Strait (e.g., *Kwok et al.*, 2004) is expected. It is worth noting that the model does not include any parameterization of landfast sea ice. We suppose that the fine mesh resolution along the coastline allows the influence of the no-slip boundary condition to vanish rapidly, resulting in a steep variation of the velocity profile. We also note in the simulation the too large ice tongue south of Fram Strait.

Fig. 6 compares the mean ice concentrations from our simulation to those derived from SMMR and SSM/I data sets (http://nsidc.org, *Comiso* (1999)) and interpolated on the finite element

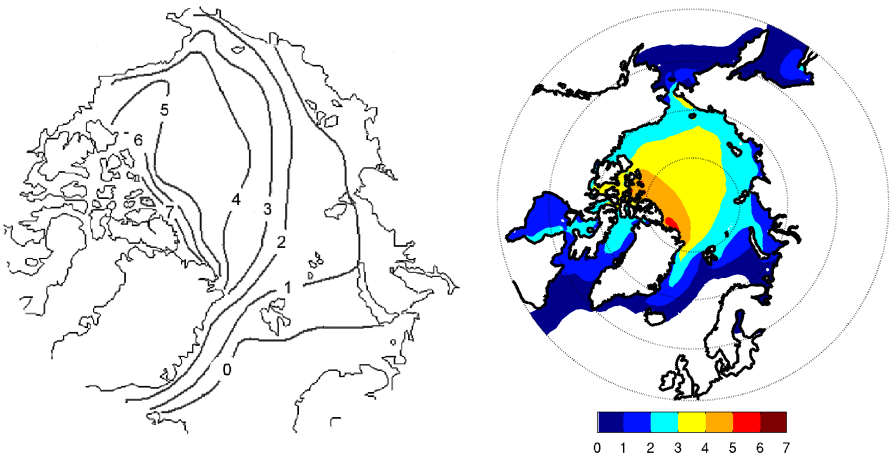

Figure 7: Global sea ice thickness pattern (in m) as computed by the model (March 1979-2005, right) and as observed (Januari-April 1960-1982, left, *Bourke and Garrett* (1987)).

mesh. As can be seen from the observations, in winter, the ice is very concentrated in the Arctic Basin ($> 90\%$) and drops near the ice edge. The simulated ice pack represents this feature, but the ice is too extensive in the southernmost part of the domain. The simple thermodynamics and parameterization of the oceanic heat flux are clearly responsible for this overestimation. In the North Atlantic, a huge amount of heat is brought into the Nordic Seas by the North Atlantic Drift Current that originates from the Gulf Stream. This feature is not present in our simulation and mostly explains the too large presence of sea ice in the Norwegian and Labrador Seas. In summer, only the central Arctic Basin remains ice-covered. The simulated ice concentration better matches the observations, even if the model still overestimates the ice cover, especially in Baffin Bay and the Kara Sea.

Finally, there is a general agreement between the simulated ice thicknesses and observations (Fig. 7). In the model central Arctic, ice thickness lies between 3 and 4 m. Thickness progressively increases from Siberia to the CAA "*providing natural barriers to the movement of the ice*" (*Bourke and Garrett*, 1987), where thickness reaches up to 6 m. The essential of the ice ridging occurs indeed in front of the CAA. Inside the CAA, some spots attain about 7 m (Fig. 10). The influence of resolving the narrow straits constituting the CAA will be investigated in a separate subsection.

4.2 Polynya formation

A polynya is "any non-linear shaped opening enclosed in ice" (*WMO*, 1970). A recent review of polynyas by *Morales Maqueda et al.* (2004) classifies them into two categories: shelf water polynyas, which are essentially mechanically driven, and deep water polynyas, thermally driven. Though spatially sparse, polynyas play a crucial role at the interface between ocean and atmosphere. On the one hand, they enable important oceanic heat losses and modify the surface albedo. On the other hand, they are at the origin of new ice formation and thus of associated brine rejection, which combined to the cooled ocean surface can lead to vertical mixing, convection and possibly to dense water production.

Most of the current coupled sea ice-ocean models do not have enough resolution to allow for polynya formation and, as a consequence, this process is either ignored or parameterized (*Morales Maqueda et al.*, 2004). Climatological results as computed by our model of the ice concentration in March (Fig. 6) reveal some areas in the domain where the concentration is decreasing in the wake of islands such as Svalbard and Novaya Zemlya, or along the eastern Siberian coast (Sea of Okhotsk). As no polynya parameterization is included in the model, this

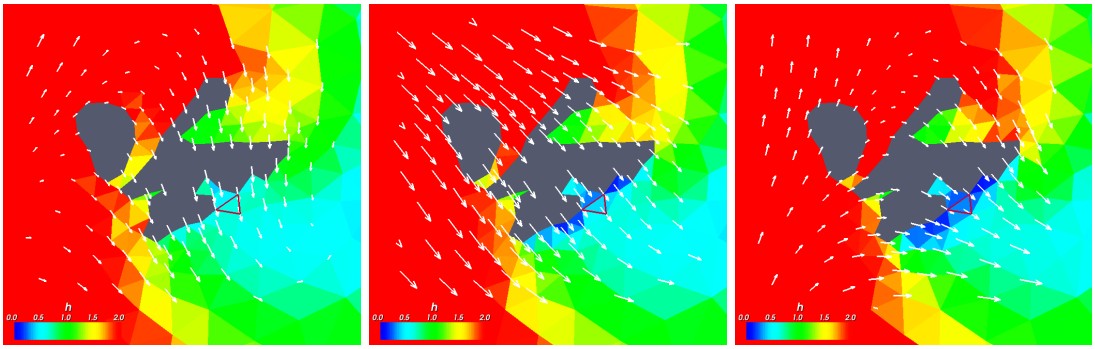

Figure 8: Formation of a wind-driven polynya in the west of the archipelago of Svalbard. Figures show the mean ice thickness (ranging from 0 to 2 m) for early March 2003 (1st, 6th and 11th, respectively). Vectors represent the wind velocity field in the area of Svalbard. The mean ice thickness and concentration of the element with red edges rapidly diminish over the 10 days from $(h, A) = (0.61$ m, 0.84) to (0.39 m, 0.57) and finally (0.26 m, 0.46).

suggests in some way a naturally induced polynya formation due to the high mesh resolution in these areas.

In order to highlight the benefits from mesh refinement, Fig. 8 illustrates the formation of a shelf water polynya west of the Svalbard archipelago during 10 days. All the conditions for shelf water polynya formation are present in our model: first, the mesh is refined around the fjord situated in the Spitsbergen island and enables the winds to export ice; second, during the 10 days between 1st and 11th March 2003, the wind direction is oriented offshore and the air temperature is about 10-15 degrees below zero. Focusing on the element with red edges shows a rapid decrease in ice concentration and thickness. On 1st March, the "initial" state yields a 0.61 m mean ice thickness with a 84% concentration. In 5 days, the ice features drop to 0.39 m and 54%, thus measuring the ice opening. Another 5 days later, the fjord and all the shelf water offshore the island are ice-covered for less than 50 % with a very thin ice layer. Finally, a couple of days later (not shown), as the wind direction is changing, the mechanical effect of the wind vanishes and sea ice thickens back in the surroundings of the fjord.

The results presented here must be cautiously considered within our general framework and hypothesis. For instance, the coarse resolution wind forcing might be not sufficient to represent accurately the wind stress in the surroundings of Svalbard. However, the aim of this subsection is to show how promising the results are regarding the possible evolution of the representation of the physical processes in the model (ice thickness distribution, a more realistic ocean feedback, more sophisticated thermodynamics, etc.) together with higher mesh refinement. Above all, they suggest polynyas might be resolved in some way without any extra parameterization.

4.3 Sensitivity experiment

In order to explore the sensitivity of the sea ice cover to the resolution of the narrow straits of the CAA, two numerical experiments are conducted. The first one (OP) corresponds to the control simulation with the CAA open. In the second experiment (CL), the straits connecting the Arctic Basin to the CAA are closed. For this purpose, the edges of the mesh crossing those straits are converted to land boundaries, thereby disconnecting the Arctic Basin from the CAA. This finally reduces to imposing a zero velocity for the velocity nodes situated on the edges in red (see Fig. 9). This procedure is meant to mimic the situation encountered in coarse resolution sea ice models that are not able to represent the exchanges of sea ice through the CAA.

Fig. 10 illustrates the climatological ice thicknesses in March for (OP) and (CL) minus (OP). As mentioned earlier, the mean ice thickness reaches about 6 m along the CAA. Inside the CAA,

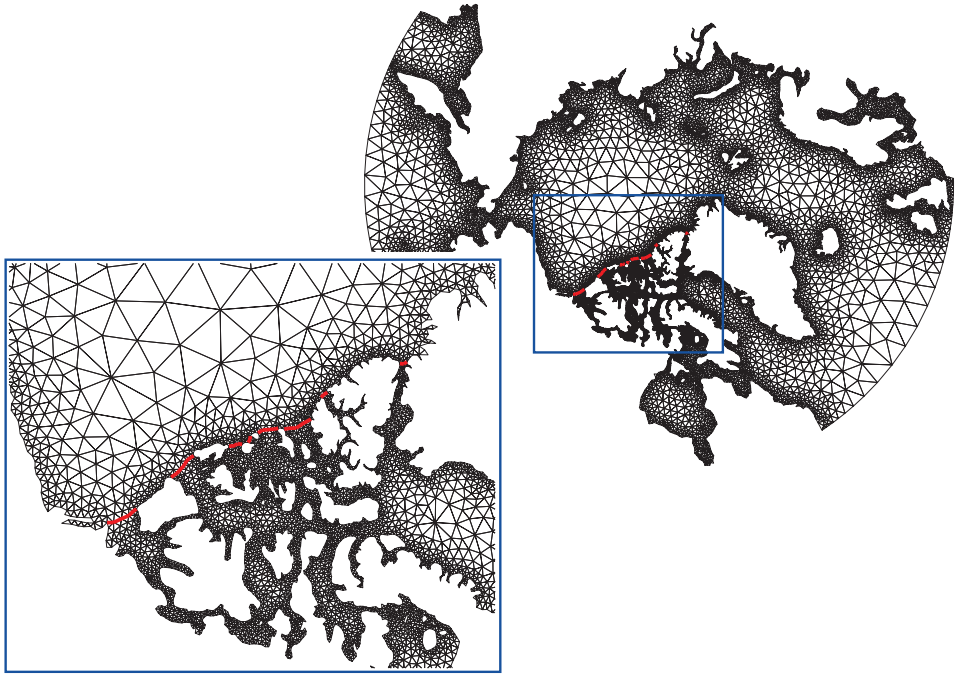

Figure 9: Zoom on the CAA. The edges in red are considered as land in the (CL) experiment, thereby closing artificially the Arctic Basin in the Canadian area.

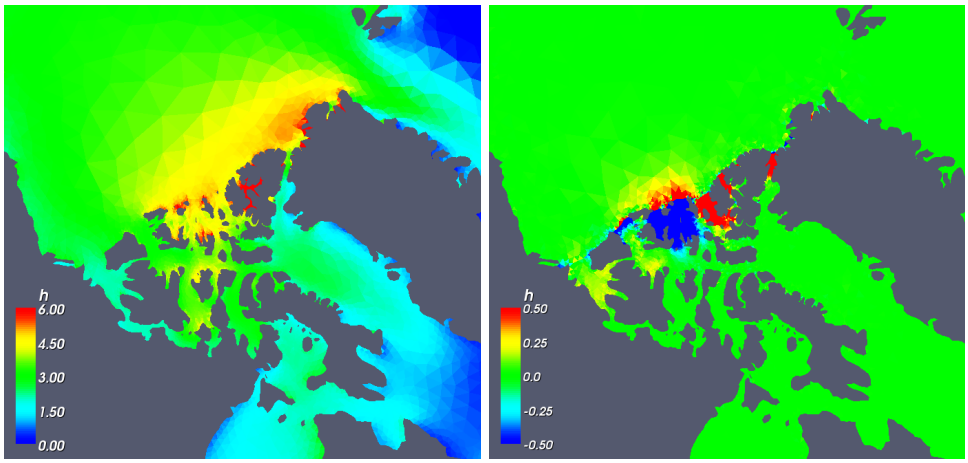

Figure 10: March ice thicknesses in the CAA for the 1979-2005 period. On the left: control simulation (OP), the scale ranges from 0 to 6 m; on the right: difference between (CL) and (OP), the scale ranges from -0.5 m to 0.5 m.

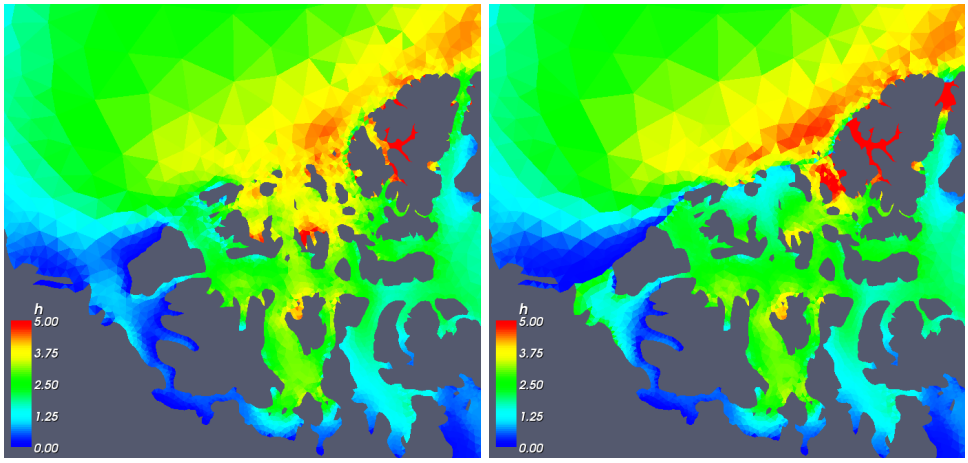

Figure 11: Ice thicknesses (from 0 to 5 m) in the CAA simulated by the model for late October 2005. On the left: control simulation (OP); on the right: (CL). Note the formation of open water in the Beaufort Sea for simulation (CL) and the difference in thickness between (OP) and (CL) along the Queen Elizabeth Islands.

thickness progressively decreases southward in direction of Baffin Bay and the Labrador Sea. What strikes first when analyzing the difference between (CL) and (OP) is the high similitude between results of both experiments. Outside a restricted area surrounding the CAA entrance, there is no clear difference between (OP) and (CL). Henceforth, on a climatological time scale, this experiment tends to attest that closing the CAA does not significantly alter the general ice thickness pattern. Nevertheless, the local thickness pattern shows a clear sensitivity to the resolution of the narrow straits north of Canada. In particular, the ice thickness difference between (OP) and (CL) is up to 2 m (not shown) in the southern gates of the Queen Elizabeth Islands (QEI-South, see *Kwok* (2006)), because of the stopped ice flux from the Arctic to the CAA.

On a daily basis, the comparison between (OP) and (CL) reveals stronger differences. The mean ice thickness patterns are compared for late October 2005 in Fig. 11. During that period, the wind is blowing offshore the CAA. Two points are to be outlined here. First, along the Queen Elizabeth Islands, the ice divergence caused by the wind is much more marked in (CL) because the closed straits prevent any ice thickness outflow from the CAA. The influence of the domain boundary and the related boundary condition diffuses inside the domain. Moreover, even a very thick ice cover, which is supposed to have a high ice strength, is very sensitive to the wind direction. In a few days, the mean ice thickness along the CAA has decreased by more than 2 m. It is worth mentioning that, in *Hibler* (1979)'s model, no tensile strength is applied to the ice and that no landfast parameterization is included in our model. The ice accumulated against the CAA is hence more sensitive to the wind direction in the (CL) experiment. Second, for the same reason, closing Amundsen Bay (southern strait in Fig. 9) in (CL) leads to an ice accumulation inside the CAA, while in Amundsen Bay it generates a large open water area, with all the physical processes concerned. The ice fluxes between both regions are thus important to accurately represent the ice flow in northern Canada.

Exchanges of sea ice between the CAA and the Arctic are extensively described and quantified by *Kwok* (2006). The model shows a good agreement with these ice fluxes (not shown here), with typically the same order of magnitude for the annual exports, except for Nares Strait and QEI-South. As expected, Nares Strait monthly ice area fluxes are weak on average (< 200 km^2), but with large northward exports for a couple of months, yielding a final Arctic inflow. The ice flux through QEI-South is too large, especially in winter when the model is clearly missing the landfast sea ice. In the next subsection, we investigate the influence of those ice fluxes on the

freshwater budget of the Arctic.

4.4 Importance of the CAA for the mass balance of Arctic sea ice

The resolution of the CAA still constitutes in the large majority of sea ice models a missing peace of the Jigsaw puzzle. In order to evaluate the importance of the CAA for the mass balance of Arctic sea ice, we perform two additional analyses in the control run (OP). First, the sea ice volume in the CAA is computed by summing the contributions of all the elements situated inside a restricted area defined by a triangle (see Fig. 12) supposed to englobe the whole CAA. According to our model, the mean CAA ice mass represents a rough 10 % of the total simulated sea ice volume, which is far from being negligible.

Second, the ice volume fluxes towards Baffin Bay are evaluated at three gates described in Fig. 12 and situated in Lancaster Sound, Jones Sound and Smith Sound. The fluxes experience a strong interannual variability and, except for three years in Lancaster Sound, contribute to a positive ice flux to Baffin Bay. As expected, Smith Sound yields the major contribution with roughly 70 % of the mean total sea ice export, while Lancaster and Jones Sounds contribute to 20 % and 10 %, respectively. Converted into mean annual freshwater fluxes, we find a contribution of $\sim$ 20 km^3 yr^{-1} for Lancaster Sound, $\sim$ 15 km^3 yr^{-1} for Jones Sound and $\sim$ 90 km^3 yr^{-1} for Smith Sound. The mean total sea ice export towards Baffin Bay is hence of 125 km^3 yr^{-1}, which is close to the 160 km^3 yr^{-1} estimated by *Prinsenberg and Hamilton* (2005).

5 Conclusions

In this paper, we have presented a finite element, unstructured grid sea ice model. The model includes a viscous-plastic rheology along with a complete parametrization of the atmospheric fluxes and is driven by daily NCEP/NCAR reanalysis data. The climatological sea ice drifts, thicknesses and concentrations computed by the model compare qualitatively well with the observations. The finite element method presented in this paper reveals effectiveness for sea ice modeling and enables the use of unstructured grids with all their potential and flexibility. In particular, higher mesh resolution in the vicinity of the coastline and islands allows for capturing small-scale processes, such as the formation of shelf water polynyas. We have shown such an example in the Svalbard Archipelago, where an offshore-oriented wind along with fine mesh resolution yields a rapid decrease in the ice thickness and concentration on a 10-days period. Such features are also noticeable on climatological concentration patterns computed by our model.

Another advantage of unstructured grids is to enable the resolution of the narrow straits of the Canadian Arctic Archipelago (CAA). A numerical experiment has been performed to investigate the influence of the ice flow through the CAA. Focusing on the large-scale sea ice thickness pattern, within our general framework and hypothesis, we have shown that the inclusion of those straits is not essential, the impact being merely local. This tends to validate the idea of the role of the CAA as a "buffer" on sea ice between the Arctic Basin and Baffin Bay. However, we have first emphasized that the local and short-term influences of the ice exchanges are nonnegligible. In particular, depending whether the straits are open or closed in the numerical experiment, the domain boundary and the associated boundary condition influence directly the numerical solution in the proximity of those straits. Second, on average, the sea ice volume in the CAA represents a nonnegligible 10 % of the total sea ice volume in our model. Furthermore, the annual sea ice volume flux towards Baffin Bay has been evaluated in order to assess its importance in the freshwater balance of the Arctic and yields a mean outflow of 125 km^3 yr^{-1}. Our estimate is in good agreement with the 160 km^3 yr^{-1} suggested by *Prinsenberg and Hamilton* (2005). All these diagnoses show how important the CAA is on the mass balance of the Arctic sea ice and plead for the need to better understand the complex processes and interactions being held in this region.

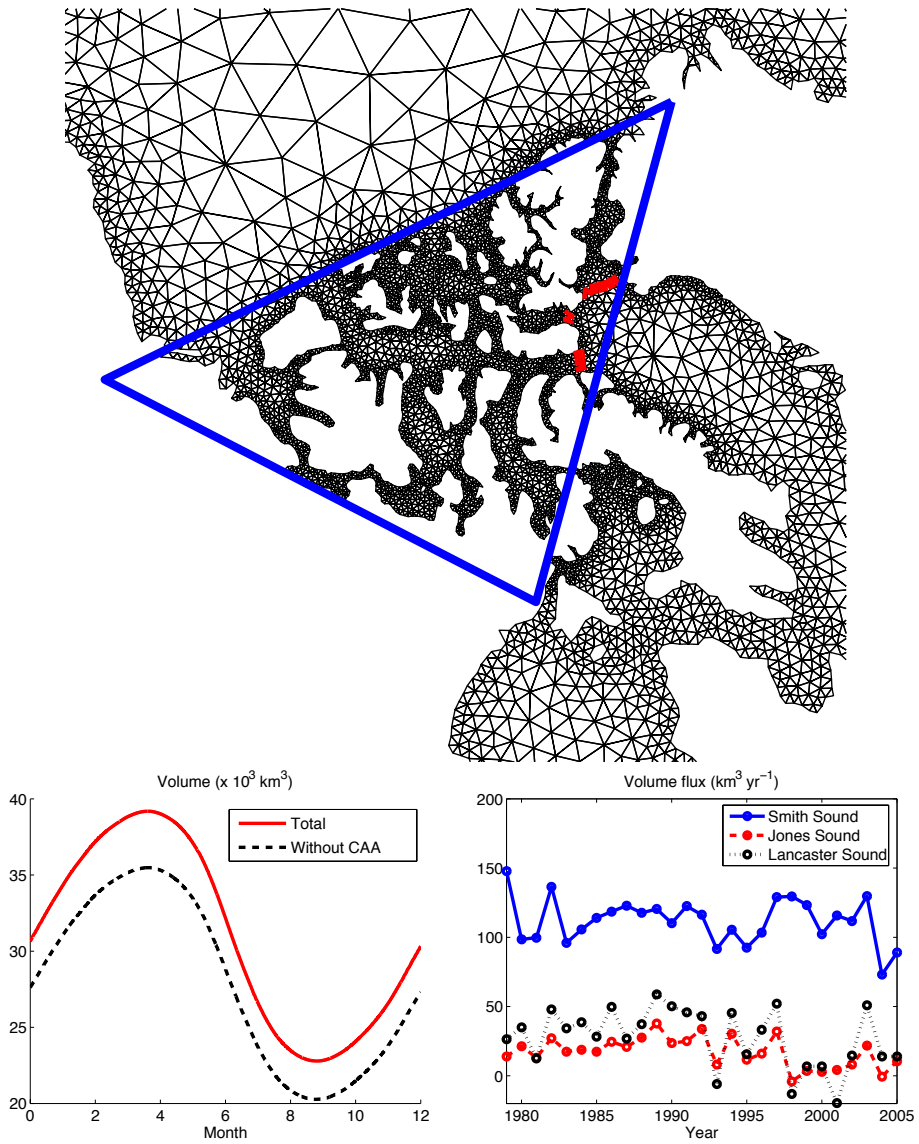

Figure 12: Top: close-up view of the mesh in the CAA. Bottom left: seasonal cycles of the Arctic sea ice volume with (solid) and without (dashed) the contribution of the CAA. Bottom right: annual ice volume fluxes (positive if directed towards Baffin Bay) through the three gates represented in the upper figure (bottom-up: Lancaster Sound, Jones Sound and Smith Sound). All the elements included in the triangle in the upper figure are considered being part of the CAA.

The results presented in this study must be considered with some care though since no ocean dynamics nor oceanic feedback are included in this uncoupled version of the model. Additionally, the *Semtner* (1976) zero-layer model is known to overestimate the seasonal variability in ice thickness (e.g., *Zhang and Rothrock*, 2001). The deficiencies of the model, including the overestimation of the simulated sea ice extent and the Bering outflow, are to be attributed to these factors. An important issue addressed by *Sou* (2007) is to know whether or not the coarse resolution atmospheric forcings typically used in the models is sufficiently accurate to enable realistic simulations in the CAA. As stated by *Wang et al.* (2003), high resolution atmospheric forcing fields might help to solve this issue. Another open question concerns the mesh resolution needed for resolving the CAA versus the continuum assumption inherent of the viscous-plastic rheology.

Some additional investigation based on a coupled sea ice-ocean model should be carried out to assess the actual role of sea ice passing through the CAA on the global ocean circulation, by way of the interactions between the associated freshwater flux and the water mass properties of the adjacent seas. Recently, this issue has been readdressed by *Kwok* (2005) concerning the impact of the ice export through Nares Strait and more generally from the CAA on the convective overturning downstream in the Labrador Sea.

Future work on the sea ice model will include a better representation of the sea ice physics (halo-thermodynamic model (*Vancoppenolle et al.*, 2007), ice-thickness distribution (*Thorndike et al.*, 1975), etc.). A coupled unstructured grid ice-ocean model might enable to assess the role of the ice fluxes through the CAA, explain the formation of static arches or propose lacking data (such as thickness order of magnitude for estimations of mass budgets). As outlined by *Dickson et al.* (2007), numerical models have indeed a role to play to make up for the inherent difficulties and financial limitations to collect data, and in particular ocean fluxes. Finally, the *Hibler* (1979) sea ice rheology imposes a zero tensile strength. We have shown that, with our model, we are not able to represent static landfast sea ice in the North Canadian Archipelago. This issue might be resolved by including some parameterization of the landfast sea ice in the model. However, detailed bathymetry and well-resolved coastal currents are needed for an appropriate simulation of landfast sea ice (*Wang et al.*, 2003). Hence, it appears that, instead of adding new features and parameterizations to the actual model, significant improvements might be gained by investigating a new rheology integrating recent laboratory research work on the mechanical properties of the ice and observations based on buoys tracking (e.g., *Schreyer et al.*, 2006; *Coon et al.*, 2007; *Weiss et al.*, 2007).

Acknowledgements

We thank Sylvain Bouillon, Valérie Dulière and Martin Vancoppenolle for inspiring discussions. The present study was carried out within the scope of the project "A second-generation model of the ocean system", which is funded by the *Communauté Française de Belgique*, as *Actions de Recherche Concertées*, under contract ARC 04/09-316. This work is a contribution to the construction of SLIM, the Second-generation Louvain-la-Neuve Ice-ocean Model (http://www.climate.be/SLIM).

References

Aagaard, K. A., and E. C. Carmack (1989), The role of sea ice and other fresh water in the Arctic circulation, *J. Geophys. Res.*, *94*, 14485–14498.

Adcroft, A., and D. Marshall (1998), How slippery are piecewise-constant coastlines in numerical ocean models?, *Tellus*, *50A (1)*, 95–108.

Arzel, O., T. Fichefet, and H. Goosse (2006), Sea ice evolution over the 20th and 21st centuries as simulated by current AOGCMs, *Ocean Modelling*, *12*, 401–415.

Becker, E. B. (1976), The finite element method in AIDJEX, *AIDJEX Bulletin*, *33*, 144–157.

Berliand, M. E., and T. G. Berliand (1952), Determining the net long-wave radiation of the Earth with consideration of the effect of cloudiness, *Isv. Akad. Nauk SSSR Ser. Geophys*, *1* (in Russian).

Berliand, M. E., and T. G. Strokina (1980), Global distribution of the total amount of clouds, Hydrometeorological Publishing House, Leningrad, Russia, 71 pp (in Russian).

Bourke, R. H., and R. P. Garrett (1987), Sea ice thickness distribution in the Arctic Ocean, *Cold Regions Science and Technology*, *13*, 259–280.

Comiso J. (1999, updated 2005), Bootstrap sea ice concentrations for NIMBUS-7 SMMR and DMSP SSM/I, June to September 2001. Boulder, CO, USA: National Snow and Ice Data Center. Digital media.

Connolley, W. M., J. M. Gregory, E. Hunke, and A. J. McLaren (2004), On the consistent scaling of terms in the sea-ice dynamics equation, *J. Phys. Oceanogr.*, *34*(7), 1776–1780.

Coon, M., R. Kwok, G. Levy, M. Pruis, H. Schreyer, and D. Sulsky (2007), Arctic Ice Dynamics Joint Experiment (AIDJEX) assumptions revisited and found inadequate, *J. Geophys. Res.*, *112*, C11S90, doi:10.1029/2005JC003393.

Danilov, S., G. Kivman, and J. Schröter (2004), A finite-element ocean model: principles and evaluation, *Ocean Modelling*, *6*, 125–150.

Dickson, R., B. Rudels, S. Dye, M. Karcher, J. Meincke, and I. Yashayaev (2007), Current estimates of freshwater flux through Arctic and subarctic seas, *Progress in Oceanography*, *73*, 210–230.

Ebert, E. E., and J. A. Curry (1993), An intermediate one-dimensional thermodynamic sea ice model for investigating ice-atmosphere interactions, *J. Geophys. Res.*, *98*(C6), 10085–10109.

Fichefet, T., H. Goosse, and M. A. Morales Maqueda (1998), On the large-scale modeling of sea ice-ocean interactions. In: *Ocean Modeling and Parameterization*, E.P. Chassignet, and J. Verron (Eds.), *NATO ASI Series*, C516, Kluwer Academic Pub., Dordrecht, pp. 399-422.

Fowler C. (2003), Polar Pathfinder Daily 25 km EASE-Grid Sea Ice Motion Vectors, Boulder, CO, USA: National Snow and Ice Data Center. Digital media.

Goosse, H., T. Fichefet, and J.-M. Campin (1997a), The effects of the water flow through the Canadian Archipelago in a global ice-ocean model, *Geophys. Res. Lett.*, *24*, 1507–1510.

Goosse H. (1997b), Modelling the large scale behaviour of the coupled ocean–sea-ice system, Ph.D. Thesis, Université catholique de Louvain, Louvain-la-Neuve, Belgium, 231 pp.

Hanert, E., D. Y. Le Roux, V. Legat, and E. Deleersnijder (2004), Advection schemes for unstructured grid ocean modelling, *Ocean Modelling*, *7*, 39–58.

Hibler, W. D. (1979), A dynamic thermodynamic sea ice model, *J. Phys. Oceanogr.*, *9*, 815–846.

Hibler, W. D. (1980), Sea ice growth, drift and decay, In *Dynamics of Snow and Ice masses*, ed. S. C. Colbeck, Academic Press, New York, 141–209.

Holland, M. M., and C. M. Bitz (2003), Polar amplification of climate change in coupled models, *Climate Dynamics*, *21*, 221–232.

Hua, B., and F. Thomasset (1984), A noise-free finite element scheme for the two-layer shallow water equations, *Tellus*, *36A*, 157–165.

Johnson, M., S. Gaffigan, E. Hunke, and R. Gerdes (2007), A comparison of Arctic Ocean sea ice concentration among the coordinated AOMIP model experiments, *J. Geophys. Res.*, *112*, C04S11, doi:10.1029/2006JC003690.

Kliem, N. and D. A. Greenberg (2003), Diagnostic simulations of the summer circulation in the Canadian Arctic Archipelago, *Atmos. Ocean*, *41*(4), 273–289.

Kwok, R., G. F. Cunningham, and S. S. Pang (2004), Fram Strait sea ice outflow, *J. Geophys. Res.*, *109*, C01009, doi:10.1029/2003JC001785.

Kwok, R. (2005), Variability of Nares Strait ice flux, *Geophys. Res. Lett.*, *32*, L24502, doi: 10.1029/2005GL024768.

Kwok, R. (2006), Exchange of sea ice between the Arctic Ocean and the Canadian Arctic Archipelago, *Geophys. Res. Lett.*, *33*, L16501, doi:10.1029/2006GL027094.

Lefebvre, W., and H. Goosse (2008), Analysis of the projected regional sea-ice changes in the Southern Ocean during the 21st century, *Clim. Dyn.*, *30*, 59–76, doi:10.1007/s00382-007-0273-6.

Legrand, S., E. Deleersnijder, E. Hanert, V. Legat, and E. Wolanski (2006), High-resolution, unstructured meshes for hydrodynamic models of the Great Barrier Reef, Australia, *Estuarine, Coastal and Shelf Science*, *68*, 36–46.

Le Roux, D. Y., C. A. Lin, and A. Staniforth (2000), A semi-implicit semi-lagrangian finite-element shallow-water ocean model, *Monthly Weather Review*, *128*, 1384–1401.

Lynch, D. R., J. T. C. Ip, C. E. Naimie, and F. E. Werner (1996), Comprehensive coastal circulation model with application to the Gulf of Maine, *Continental Shelf Research*, *16*, 875–906.

Manabe, S., and R. J. Stouffer (1980), Sensitivity of a global climate model to an increase of CO2 concentration in the atmosphere, *J. Geophys. Res.*, *85*(C10), 5529–5554.

Melling, H. (2002), Sea ice of the northern Canadian Arctic Archipelago, *J. Geophys. Res.*, *107*(C11), 3181, doi:10.1029/2001JC001102.

Morales Maqueda, M. A., A. J. Willmott, and N. R. T. Biggs (2004), Polynya Dynamics: a Review of Observations and Modeling, *Rev. Geophys.*, *42*, RG1004, doi:10.1029/2002RG000116.

Mukherji, B. (1973), Crack propagation in sea ice: a finite element approach, *AIDJEX Bulletin*, *18*, 69–75.

Perovich, D. K., T. C. Grenfell, B. Light, and P. V. Hobbs (2002), Seasonal evolution of the albedo of multiyear Arctic sea ice, *J. Geophys. Res.*, *107*(C10), 8044, doi: 10.1029/2000JC000438.

Pietrzak, J., E. Deleersnijder, and J. Schröter (2005), The Second International Workshop on Unstructured Mesh Numerical Modelling of Coastal, Shelf and Ocean Flows, *Ocean Modelling*, *10*, 1–252, (special issue).

Prinsenberg, S. J., and J. Hamilton (2005), Monitoring the volume, freshwater and heat fluxes passing through Lancaster Sound in the Canadian Arctic Archipelago, *Atmos. Ocean*, *43*, 1–22.

Samelson, R. M., T. Agnew, H. Melling, and A. Münchow (2006), Evidence for atmospheric control of sea-ice motion through Nares Strait, *Geophys. Res. Lett.*, *33*, L02506, doi:10.1029/2005GL025016.

Schreyer, H. L., D. L. Sulsky, L. B. Munday, M. D. Coon, and R. Kwok (2006), Elastic-decohesive constitutive model for sea ice, *J. Geophys. Res.*, *111*, C11S26, doi:10.1029/2005JC003334.

Schulkes, R. M. S. M., L. W. Morland, and R. Staroszczyk (1998), A finite-element treatment of sea ice dynamics for different ice rheologies, *International Journal for Numerical and Analytical Methods in Geomechanics*, *22*, 153–174.

Semtner, A. J. (1976), A model for the thermodynamic growth of sea ice in numerical investigations of climate, *J. Phys. Oceanogr.*, *6*, 379–389.

Serreze, M. C., R. G. Barry, and A. S. McLaren (1989), Seasonal variations in sea ice motion and effects on sea ice concentration in the Canada Basin, *J. Geophys. Res.*, *94*, 10955–10970.

Serreze, M. C., A. P. Barrett, A. G. Slater, R. A. Woodgate, K. Aagaard, R. B. Lammers, M. Steele, R. Moritz, M. Meredith, and C. M. Lee (2006), The large-scale freshwater cycle of the Arctic, *J. Geophys. Res.*, *111*, C11010, doi:10.1029/2005JC003424.

Serreze, M. C., M. M. Holland, and J. Stroeve (2007), Perspectives on the Arctic's shrinking sea-ice cover, *Science*, *315*, 1533–1536, doi:10.1126/science.1139426.

Sodhi, D. S., and W. D. Hibler (1980), Nonsteady ice drift in the Strait of Belle Isle, In: Pritchard, R. S. (Ed.), *Sea Ice Processes and Models*. University of Washington Press, Seattle and London, 177–186.

Sou T. V. (2007), The flow and variability of sea-ice in the Canadian Arctic Archipelago: modelling the past (1950-2004) and the future (2041-2060), Master Thesis, University of Victoria, Victoria, Canada, 125 pp.

Steele, M., R. Morley, and W. Ermold (2001), PHC: A global ocean hydrography with a high quality Arctic Ocean, *J. Climate*, *14*, 2079–2087.

Stigebrandt, A. (2000), Oceanic freshwater fluxes in the climate system. In: *The freshwater budget of the Arctic Ocean*, Kluwer Acad. Publ., New York, 1–20.

Stroeve, J., M. C. Serreze, F. Fetterer, T. Arbetter, W. Meier, J. Maslanik, and K. Knowles (2005), Tracking the Arctic's shrinking ice cover: Another extreme September minimum in 2004, *Geophys. Res. Lett.*, *32*, L04501, doi:10.1029/2004GL021810.

Stronach, J. A., J. A. Helbig, S. S. Salvador, H. Melling, and R. A. Lake (1987), Tidal elevations and tidal currents in the Northwest Passage, *Can. Tech. Rep. Hydrogr. Ocean Sci.*, *97*, Inst. of Ocean Sci., Sidney, B.C., 329 pp.

Sulsky D., H. Schreyer, K. Peterson, R. Kwok, and M. Coon (2007), Using the material-point method to model sea ice dynamics, *J. Geophys. Res.*, *112*, C02S90, doi:10.1029/2005JC003329.

Thomson, N. R., J. F. Sykes, and R. F. McKenna (1988), Short-term ice motion modeling with application to the Beaufort Sea, *J. Geophys. Res.*, *93*, 6819–6836.

Thorndike, A. S., D. A. Rothrock, G. A. Maykut, and R. Colony (1975), The thickness distribution of sea ice, *J. Geophys. Res.*, *80*, 4501–4513.

Thorndike, A. S. and R. Colony (1982), Sea ice motion in response to geostrophic winds, *J. Geophys. Res.*, *87*, 5845–5852.

Timmermann, R., H. Goosse, G. Madec, T. Fichefet, C. Ethe, and V. Dulière (2005), On the representation of high latitude processes in the ORCA-LIM global coupled sea ice-ocean model, *Ocean Modelling*, *8*, 175–201.

Trenberth, K. E., J. G. Olson, and W. G. Large (1989), A global ocean wind stress climatology based on ECMWF analyses, National Center for Atmos. Res., NCAR/TN-338+STR, Boulder, Colorado, 93 pp.

Vancoppenolle, M., C. M. Bitz, and T. Fichefet (2007), Summer landfast sea ice desalination at Point Barrow, Alaska: Modeling and observations, *J. Geophys. Res.*, *112*, C04022, doi: 10.1029/2006JC003493.

Vancoppenolle, M., T. Fichefet, H. Goosse, S. Bouillon, and M. A. Morales Maqueda (subm.), Modeling global sea ice and its salinity in OPA9-LIM3, an ice-ocean model. 1. Model description and validation, *Ocean Modelling*, *subm.*

Wallace, J. M. and P. V. Hobbs (1977), Atmospheric Science: An Introductory Survey, *Academic Press*, 467 pp.

Walters, R. A. (1992), A three-dimensional, finite element model for coastal and estuarine circulation, *Continental Shelf Research*, *12*, 83–102.

Wang, J., R. Kwok, F. J. Saucier, J. Hutchings, M. Ikeda, W. Hibler, J. Haapala, M. D. Coon, H. E. Markus Meier, H. Eicken, N. Tanaka, D. Prentki, and W. Johnson (2003), Working toward improved small-scale sea ice-ocean modeling in the Arctic Seas, *Eos*, *84*(34), 325–336.

Wang, L. R., and M. Ikeda (2004), A Lagrangian description of sea ice dynamics using the finite element method, *Ocean Modelling*, *7*, 21–38.

Weiss, J., E. M. Schulson, and H. L. Stern (2007), Sea ice rheology from in-situ, satellite and laboratory observations: Fracture and friction, *Earth and Planetary Science Letters*, *255*, 1–8.

White, L., V. Legat, and E. Deleersnijder (2008a), Tracer conservation for three-dimensional, finite element, free-surface, ocean modeling on moving prismatic meshes, *Monthly Weather Review* (in press), doi:10.1175/2007MWR2137.1.

White, L., E. Deleersnijder, and V. Legat (2008b), A three-dimensional unstructured mesh finite element shallow-water model, with application to the flows around an island and in a wind-driven, elongated basin, *Ocean Modelling* (accepted for publication).

Williamson, D. (1979), Difference approximations for fluid flow on a sphere, In: *Numerical methods used in atmospheric models*, chapter 2, 51–120. GARP Publication Series no. 17, WMO-ICSU.

WMO (1970), WMO sea ice nomenclature, terminology, codes and illustrated glossary, *WMO/OMM/BMO-No. 259*, T.P. 145, 147 pp + 8 suppl., Geneva, Switzerland.

Yakovlev, N. G. (2003), Coupled model of Ocean General Circulation and sea ice evolution in the Arctic Ocean, *Izvestiya, Atmospheric and Oceanic Physics*, *39*, 355–368.

Zhang, J., and D. Rothrock (2001), A Thickness and Enthalpy Distribution Sea-Ice Model, *J. Phys. Oceanogr.*, *31*, 2986–3001.

Zhang, X., and J. E. Walsh (2006), Toward a seasonally ice-covered Arctic Ocean: Scenarios from the IPCC AR4 model simulations, *J. Climate*, *19*, 1730–1747.

Zillmann, J. W. (1972), A study of some aspects of the radiation and the heat budgets of the southern hemisphere oceans, *Meteorol. Stud.*, *26*, Bur. Meteorol. Dep. of the Interior, Canberra, Australia, 562 pp.

List of Figures